Asian Journal of Pharmaceutical Sciences 14 (2019) 275–286

Available online at www.sciencedirect.com

ScienceDirect

journal homepage: www.elsevier.com/locate/AJPS

Original Research Paper

MSNCs and MgO-MSNCs as drug delivery systems to control the adsorption kinetics and release rate of indometacin

Xin Zheng[a,b], *Shuang Feng*[a], *Xiudan Wang*[a], *Zhenning Shi*[a], *Yuling Mao*[a], *Qinfu Zhao*[a,*], *Siling Wang*[a,*]

[a] *Department of Pharmaceutics, School of Pharmacy, Shenyang Pharmaceutical University, Shenyang 110016, China*
[b] *School of Pharmaceutical Engineering, Shenyang Pharmaceutical University, Shenyang 110016, China*

ARTICLE INFO

Article history:
Received 25 February 2018
Revised 1 August 2018
Accepted 17 August 2018
Available online 20 September 2018

Keywords:
MSNCs
MgO-MSNCs
Indometacin
Adsorption
Release rate

ABSTRACT

Mesoporous silica cocoon materials (MSNCs) and MgO doped mesoporous silica cocoons (MgO-MSNCs) with the cocoon-like hierarchical morphology and different alkalinities were synthesized as carriers for acidic drugs. Indomethacin (IMC) was selected as a model drug and loaded into carriers. All materials and the drug-loaded samples were characterized by nitrogen adsorption, FTIR spectroscopy, transmission electron microscopy (TEM), powder X-Ray diffraction (XRD) and differential scanning calorimetry (DSC). The effect of the Mg/Si molar ratio on the kinetics and equilibrium of IMC adsorption on MgO-MSNCs was thoroughly examined, and it was found that the increase in the Mg/Si molar ratio resulted in an increasing IMC adsorption rate due to the increased affinity between alkaline MgO-MSNCs and weak acid IMC. The adsorption kinetics fitted a pseudo second-order model well. The Freundlich isotherm showed a better fit, indicating that the coverage of IMC on the surface of MgO-MSNCs was heterogeneous. The maximum adsorption capacity of adsorbent was calculated by the Langmuir isotherm equation. The Temkin equation provided further support that the IMC adsorption on MgO-MSNCs was dominated by a chemisorption process. MgO-MSNCs also have the advantage of allowing an adjustment of the drug release rate of weak acid drug. The cytotoxicity assay indicated good biocompatibility of MgO-MSNCs. Our research on MgO-MSNCs carriers demonstrated their potential therapeutic benefit for safe and effective management of IMC adsorption and *in vitro* release.

* Corresponding authors at. Department of Pharmaceutics, School of Pharmacy, Shenyang Pharmaceutical University, No. 103, Wenhua Road, Shenyang 110016, China. Tel.: +86 24 43520537
E-mail addresses: zqf021110505@163.com (Q.F. Zhao), silingwang@syphu.edu.cn (S.lL Wang).
Peer review under responsibility of Shenyang Pharmaceutical University.

https://doi.org/10.1016/j.ajps.2018.08.004

1. Introduction

Generally, a successful drug delivery system needs to build a biocompatible carrier which has a high drug loading capacity and allows controlled release of the cargo when it reaches its destination [1]. Recently, mesoporous silica nanoparticles with a systematic tailorable pore architecture and the high surface area have attracted attention because of their potential use as vehicles for drug delivery [2,3]. Methods that can affect the porosity, pore morphology, pore size distribution and the morphology of the materials are of particular interest. Factors, such as the hydrolysis of silicate, the shape of the surfactant micelles, inorganic salts, organic swelling agents and co solvents, can affect the morphology of the products [4]. In the preparation of mesoporous silicates, the addition of organic swelling agents, for example, 1,3,5-trimethylbenzene (TMB), n-hexane and n-nonane, which may be soluble in the hydrophobic cores of the surfactant micelles, can lead to a larger micelle size and a greater pore diameter [5]. Apart from a pore-expanding effect, the swelling agents can also produce some changes in the morphology of the materials. For example, when the concentration of TMB is low, a hexagonally packed pore structure is achieved, and increasing the TMB/P123 ratio will produce a new mesocellular foam phase. When 1,3,5-triisopropylbenzene is used as a swelling agent, a hexagonal structure can be obtained at a low TIPB/P123 ratio while a vesicle-like silica produces a high TIPB/P123 ratio [6]. To our knowledge, the mesostructure assembly is also greatly affected by the formation of O/W emulsions, while the combination of an emulsion and a templating agent in the synthesis of mesoporous silica materials has received little attention.

Since the inorganic carriers have many favorable properties, such as a high surface area, large pore volume and tunable pore size, much research has focused on applications involving drug delivery systems [7, 8]. In addition to immediate-release, there also many research studies on controlled drug release [9]. Sun et al. have explored a novel spherical nanosilica matrix (SNM) together with chitosan encapsulated SNM to investigate the feasibility of using chitosan to regulate the drug release rate from porous silica and obtain an oral sustained drug delivery system. The dispersing effect of SNM and the swelling of chitosan were the two main factors contributing to the sustained drug release behavior. From the research described above, it appears that the dissolution rate is considered as the most important factor determining the bioavailability of orally administered poorly water-soluble drugs.

Highly basic novel mesoporous materials have been successfully produced by dispersing MgO on SBA-15 using three different methods, impregnation, microwave irradiation and a combination of these, via the magnesium acetate path [10]. Also, Wang et al. [11] have reported that MgO particles did not destroy the SBA-15 mesoporous structure after their incorporation. A few years later, there was an investigation of silica particles which were functionalized using their basic properties for the controlled release of ibuprofen with acidic groups [12]. Shen et al. [13] synthesized submicron MgO-modified SBA-15 silica. Compared with SBA-15, the amount of ibuprofen adsorbed on the MgO-modified silica was increased and the release rate from the mesoporous matrix was retarded.

In this paper, the swelling agent n-decane in an O/W emulsion-assisted self-assembly process was used to obtain novel 3-dimensional silica cocoons with a larger micelle size and, consequently, leading to a greater pore diameter. In addition, the cocoons doped with magnesia using an *in situ* one-spot method by adding magnesium nitrate to the process for synthesizing MSNCs, and then the basic mesoporous materials from the strongly acidic system were obtained. Matrices with different Mg/Si ratios were obtained for the efficient encapsulation of the acidic drug IMC and they exhibited different adsorption and release behaviors. To our knowledge, little research has been published on the investigation of the detailed adsorption characteristics of the drug adsorption kinetics and isotherm models of IMC adsorption onto such mesoporous silicon cocoons. We also used pseudo-first-order and pseudo-second-order kinetics to obtain a better understanding of the controlling reaction pathways, whether chemisorption or physisorption, and the mechanisms of surface *versus* intraparticle diffusion involved in the adsorption reactions. Kinetic data were used to predict the rate at which the drug IMC was adsorpted onto MgO-MSNCs and the equilibrium adsorption isotherms were used to quantify the adsorptive capacity of the adsorbent.

2. Materials and methods

2.1. Materials

$EO_{20}PO_{70}EO_{20}$ (Pluronic P123) was obtained from Sigma-Aldrich (St. Louis, MO, USA). Ammonium fluoride was purchased from Aladdin (Shanghai, China). Tetraethyl orthosilicate (TEOS), hydrochloric acid and magnesium nitrate hexahydrate were purchased from Yu Wang Reagent Company (Shandong, China) while n-decane was kindly donated by Fushun Beiyuan Fine Chemical Company Ltd. (Fushun, China). Indomethacin (purity > 99.0%) was kindly supplied by Shijiazhuang Pharmaceutical Group (Huasheng Pharm. Co., Ltd.). All other chemicals were of reagent grade and used as purchased without further purification.

2.2. Preparation of MSNCs and MgO-MSNCs

The preparation procedure of MSNCs was as follows: 2.5 g P123 was added to 80 ml of 1.0 M HCl solution at room temperature. After a clear solution was obtained, 7.4 g n-decane was added, and the mixture was gently stirred overnight to solubilize the cores of the P123 micelles. After stopping stirring, the P123-decane-water mixture was stand for 8 h to obtain a water-rich layer and a decane-rich layer and then 0.03 g NH_4F was added to the remaining water-rich layer. This water-rich layer was stirred at 40 °C for 15 min, followed by the dropwise addition of tetraethyl orthosilicate. The mixture was then stirred at 40 °C for 24 h and hydrothermally treated in an autoclave at 100 °C for 48 h. The product was recovered by evaporation, and re-dispersed in distilled water. After stirring at 40 °C for 2 h, filtered and washed with deionized water, then dried at 60 °C overnight. Finally, the white powder obtained was calcined at 550 °C for 6 h to remove the template agent P123.

The MgO-MSNCs were prepared by the same method, except for the addition of a different molar ratio of $Mg(NO_3)_2$•$6H_2O$ to the water-rich layer and stirred for 0.5 h before 0.03 g NH_4F was added.

2.3. Sample characterization

TEM (TECNAI G220, FEI, USA) observations provide information about the mesoporous structure of carriers. The pore volumes and size distributions were obtained using a surface area analyzer (SA3100, Beckman Coulter, USA). The method of Brunauer–Emmett–Teller (BET) was used for determining the surface area of samples. And the method of Barrett–Joyner–Halenda (BJH) was used to determine the pore size distribution. FT-IR (Bruker IFS 55, Switzerland) was used to obtain information about the characteristics of the organic groups on the surface of the samples over a spectroscopic range of 500–4000 cm^{-1}. DSC experiments were conducted using a differential scanning calorimeter (DSC 60, Shimadzu Co., Japan). Sample was heated at 10 °C/min under N_2 flow of 40 ml/min in an aluminum pan. XRD was performed on a diffractometer (PANALY IICALB.V, PW3040/60) with Cu-Kα radiation ($\lambda = 1.5405$ Å). Powder samples were scanned over the 2θ angle range from 5° to 60° with a scan rate of 5.0°/min. The basicity of the samples was measured as follow: the sample was shaken in 0.02 M hydrochloric acid solution (5 ml), and the remaining acid was then titrated by standard base (0.02 M aqueous NaOH), then the basicity of the samples was obtained by calculation.

2.4. Adsorption experiments

Different Mg/Si ratios affected the adsorption kinetics of IMC by MgO-MSCNs, and 10 mg samples of MgO-MSCNs (Mg/Si = 0, 0.4, 0.6, 0.8, 1.0) were added to EP tubes containing 2 ml IMC methanol solution. A sealing film was capped to the EP tubes to avoid methanol volatilization during the equilibration process. Experiments were carried out in a temperature controlled table concentrator. Samples were collected at 0, 10, 20, 30, 45, 60, 120, 180 and 240 min for IMC analysis. Adsorption isotherms were obtained by varying the initial IMC concentration from 0.5 to 5 mg/ml in 2 ml EP tubes with 10 mg carriers. The samples were collected at 0 and 48 h to quantify the initial and final IMC concentrations.

The IMC uptake q (mg IMC per g MgO-MSCNs) was determined by mass balance, as follows [14]:

$$q_t = (C_0 - C_t) \times V/m \quad (1)$$

Where C_0 and C_t are IMC concentrations (mg/l) at time 0 and t, respectively, V is the volume of the solution (ml), and m is the mass of MgO-MSCNs (mg).

2.5. Drug loading procedure

IMC was incorporated into the pores of MgO-MSNCs samples by an adsorption equilibrium method. In detail, the carriers and IMC/methanol (10 mg/ml) were mixed (the mass ratio of IMC to carrier was 1/3, w/w). Then, the mixture was allowed to reach adsorption equilibrium under gently stirring for 24 h at room temperature in a closed container. Finally, the mixture was centrifuged at 10 000 rpm to obtain a powder precipitate which was washed with methanol to remove residual drug on the surface of the carrier. The product was then dried at 40 °C until the organic solvent was removed. The loaded samples were referred as IMC-MSCNs and IMC-MgO-MSCNs.

2.6. In vitro study of the dissolution rate

Dissolution experiments were carried out in phosphate buffer (pH 6.2), using a USP II paddle method (75 rpm, 37 °C and 900 ml dissolution medium) with a dissolution instrument (KC-8D, Tianjin Guoming Medical Equipment Co. Ltd.). At first, IMC-loaded samples (equivalent to 20 mg IMC) were added to the dissolution medium, and then 5 ml samples of the release medium were collected and passed through a 0.22 μm membrane filter at regular intervals. Finally, the concentration of the released IMC was determined at 318 nm by UV–vis spectrophotometry (UV-2000, Unico, USA).

2.7. In vitro cytotoxicity studies

Caco-2 cells were cultured using Dulbecco's Modified Eagle's Medium (DMEM) supplemented with 10% FBS, 1% non-essential amino acids, penicillin and streptomycin. The culture was maintained at 37 °C at an atmosphere of 5% CO_2 and 95% relative humidity. To evaluate the *in vitro* cytotoxicity of the MSNCs and MgO-MSNCs nanoparticles, Caco-2 cells were seeded onto 96-well plate at a density of 2×10^4/well at 37 °C for 24 h. Subsequently, the cells treated with various concentrations of MSNCs and MgO-MSNCs carriers (20, 50, 100, 200, 500 μg/ml) for another 24 h. The cell viability was evaluated by using MTT 3-[4, 5-dimethylthiazol-2-yl]−2, 5-diphenyltetrazolium bromide) assay. Then, 20 μl MTT (5 mg/ml) solution was added into each well and further incubation for 4 h at 37 °C. Finally, the mixture was taken out and 150 μl DMSO was added into the wells to dissolve the formazan crystals produced by the living cells. The absorption of each well was measured at a wavelength of 570 nm using a microplate reader (SpectraMax M3, Molecular Devices, USA).

3. Results and discussion

3.1. Sample morphology characterization

During the preparation process of MSNCs, triblock copolymer P123 was used as a template due to its ability to self-organize into micelles. The addition of the organic swelling agent n-decane, which was soluble in the hydrophobic cores of the surfactant micelles, will produce a larger micelle size and, consequently, leading to a greater pore diameter [5]. Compared with the traditional mesoporous silica material SBA-15, which was known as a rod-shaped morphology with uniform pore size, the addition of n-decane made the structures of MSNCs become 3-dimensional cocoon-like pouches instead of 2-dimensional nano-chunks as shown in Fig. 1A and B. Therefore, n-decane might play two roles in the synthesis process. Initially, it acted as a swelling agent to produce P123 micelles with a large diameter. More importantly, n-decane

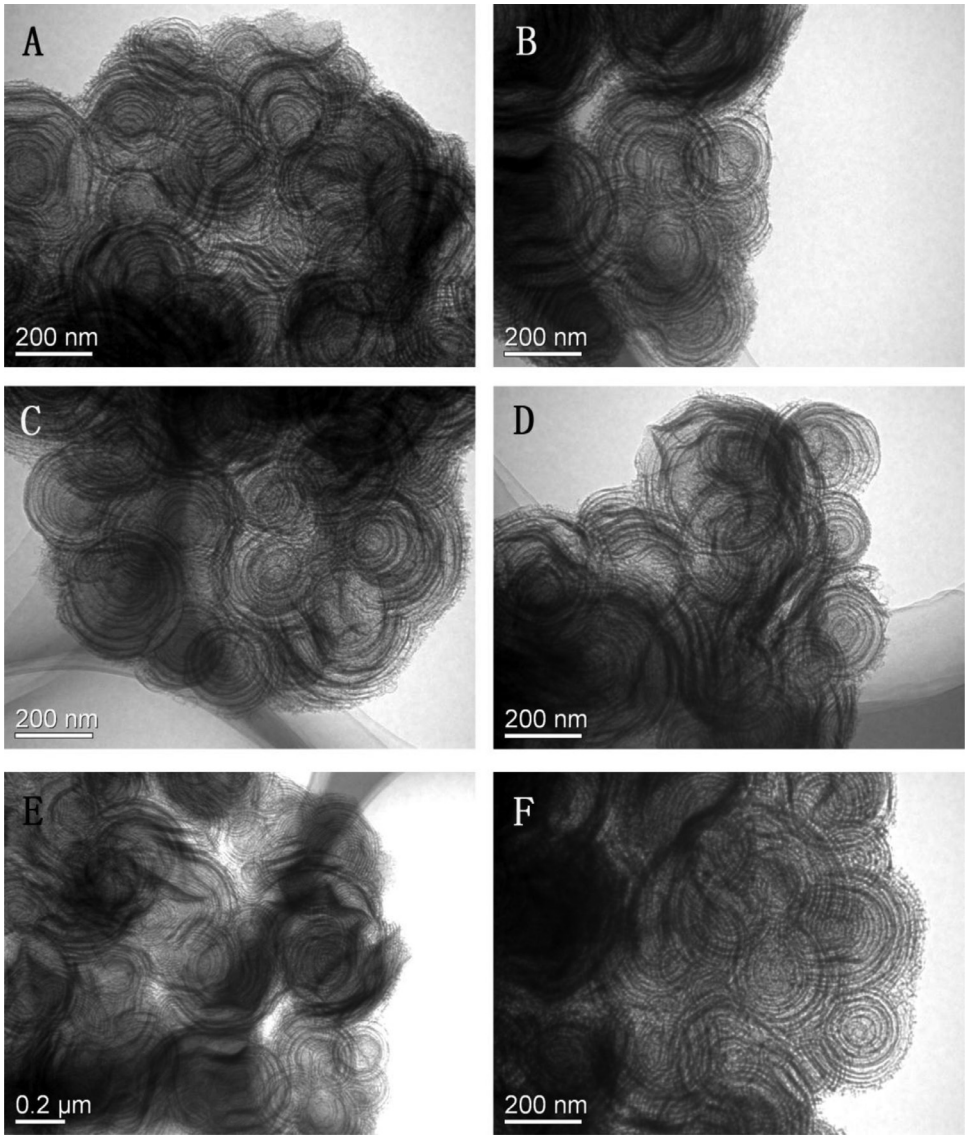

Fig. 1 – TEM images of (A, B) MSCNs, (C) 0.4MgO-MSCNs, (D) 0.6MgO-MSCNs, (E) 0.8MgO-MSCNs, and (F) 1.0MgO-MSCNs.

allowed the formation of the O/W emulsion, in which the P123 micelles aggregated to form a layer by layer structure. When the silica source (TEOS) was added to the water-rich-layer obtained, a hydrolysis reaction occurred, giving a mesostructured nanocomposite. After calcination, the triblock copolymers were removed, and the final product was obtained.

The MgO-MSNCs were prepared *in situ* by a one-spot method, in which $Mg(NO_3)_2{\cdot}6H_2O$ was added to the water-rich layer and stirred for 0.5 h before 0.03 g NH_4F was added. This resulted in basic mesoporous material being obtained from the strongly acidic system. The inner structures of MSNCs and MgO-MSNCs were characterized by TEM and the results are shown in Fig. 1. It was found that the materials are 3-dimensional cocoon-like pouches. The wall of these cocoons is curved and the ordered channels are also curved. These perspective images were due to superposition of the nanosized cocoon-like units. The TEM results indicated that the addition of the precursor salt $Mg(NO_3)_2{\cdot}6H_2O$ in synthetic process did not markedly change the mesoscopic order of the MSNCs, and the smooth MgO layers were formed on the surface of MSNCs.

Another interesting phenomenon is that magnesium oxide was obtained in a strongly acidic solution (pH < 1) without interaction, since the magnesium oxide was alkaline. But how the magnesium ions enter the curved and ordered channels of the as-made sample, this may be attributed to the mobility of P123 in the channels of the material. Since the surfactant can be easily extracted by water, it also enables Mg^{2+} cations to migrate and combine with the PEO head of P123 in the inner pores. At the same time, Mg^{2+} cation also has a chance to connect with surface silanol groups. According to the preparation procedure, when the sample was removed from the evaporation step without further drying and calcination, and re-dispersed in the distilled water, the pH value was less than 1, indicating that the large amount of HCl remained in the sample, no MgO may exist in such acidic condition. Then the mixture was continued to stir at 40 °C for 2 h, filtrated, washed with water, dried at 60 °C and calcined at

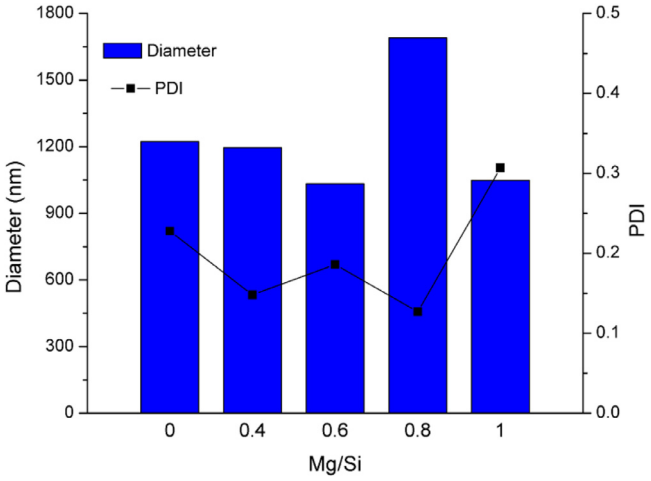

Fig. 2 – The diameter and PDI of MgO-MSCNs with different Mg/Si ratios.

550 °C. Based on these observations, incorporation of magnesium in MSNCs did not occur in the initial hydrothermal step, but probably in the evaporation step. The magnesium species survived in the strong acid solution (pH < 1), of course they were not basic or soluble but probably anchored with surface silanol groups. Once the Si–O–Mg monolayer is formed, they would be converted to an MgO layer in the calcination process, changing both the surface area and pore volume of MSCNs [15]. The 0.4MgO-MSNCs, 0.6MgO-MSNCs, 0.8MgO-MSNCs and 1.0MgO-MSNCs samples possesses a basicity of 10.69, 17.86, 21.79 and 31.94 mmol OH^-/g in titration as shown in Fig. S1, respectively. The size distribution and polydispersity index (PDI) were measured to identify the uniformity of nanoparticles as shown in Fig. 2. The diameters of MgO-MSCNs with different Mg/Si ratios were about 1000–1700 nm with the PDI less than 0.3, indicating that the carriers had the relatively uniform particle sizes.

The structures of the products were also investigated by the Brunauer–Emmett–Teller (BET) nitrogen adsorption isotherm, which is shown in Fig. 3A. From the figure, the specific surface area of the sample ranges from 478.99 m^2/g to 524.32 m^2/g, and ordered mesoporous materials with a narrow pore size distribution from 9.79 nm to 16.01 nm are suggested by the inset of Fig. 3A. Compared with the conventional SBA-15, the larger pore size is probably due to the presence of n-decane in the P123 micelles [16].

The pore diameter, surface area and total pore volume of different samples are shown in Table 1 and Fig. 3B. The surface area, total pore volume and pore diameter were all increased with an increase in the content of magnesium nitrate. This can be explained by the Hofmeister theory, in which Na^+, Cl^- and CH_3COO^- are generally salting-out ions, which can be regarded as water-structure-makers or cosmotropic ions, while Mg^{2+} and NO_3^- are salting-in ions, as we call them, water-structure-breakers or chaotropic ions [15]. Due to the salting-in nature of Mg^{2+} and NO_3^-, the added magnesium nitrate enhances the formation of the polar environment, and hinders the dehydration of PEO blocks, which promotes the formation of the hybrid interface between the silica and PEO segments,

Table 1 – Pore diameter, surface area and total pore volume of different MgO-MSCNs samples.

Different ratios	D_p (nm)	S_{BET} (m^2/g)	V_t (cm^3/g)
Mg/Si = 0	9.79	478.99	1.26
Mg/Si = 0.4	10.82	500.96	1.34
Mg/Si = 0.6	12.34	513.81	1.45
Mg/Si = 0.8	13.21	522.64	1.72
Mg/Si = 1	16.01	524.32	1.77

followed by an increase in the surface area and pore volume of MSNCs. A schematic illustration of the *in-situ* emulsion-assisted process is proposed in Scheme 1.

3.2. *Adsorption kinetics*

The adsorption of drug molecules onto porous matrix materials is determined by the pore size distribution and surface properties. The pore size of supporting carrier determines the number of drug molecules that can be adsorbed into its channels. In other words, compared with classic SBA-15 materials, more drug molecules may be adsorbed into such cocoon-like silica materials due to the larger pore size. Owing to the alkaline surface of MgO-MSCNs, it was also very useful for the acidic drug loading. The adsorption kinetics of the products was used to investigate the saturated adsorption capacity of MgO-MSCNs.

The molar ratio of Mg/Si is an important factor in the adsorption process. The effect of the molar ratio on the adsorption of IMC by MgO-MSCNs was studied from 0 to 1 at $C_0 = 2$ mg/ml and an MgO-MSCNs mass of 10 mg. As shown in Fig. 4, an increase in the molar ratio resulted in an increased IMC adsorption rate and equilibrium sorption capacity, with the equilibrium IMC adsorption increasing from 28.34 mg/g at Mg/Si = 0 to 67.94 mg/g at Mg/Si = 1, while the time required to reach sorption equilibrium was 240 min. This may be attributed to that the basicity of MgO-MSCNs was stronger at a higher molar ratio of Mg/Si, which resulted in stronger combining force interaction between MgO-MSCNs and the carbonyl group of model drugs IMC.

Parameters from two kinetic models, pseudo-first-order [17] and pseudo-second-order [18], were fitted to the experimental data to evaluate the adsorption kinetics of IMC uptake by MgO-MSCNs.

The pseudo-first-order equation describes adsorption in solid–liquid systems based on the sorption capacity of solids [17]. The linear form of the pseudo-first order model can be expressed as:

$$\log(q_e - q_t) = \log q_e - k_1 t/2.303 \quad (2)$$

Where q_e and q_t (mg/g) are the adsorption capacities at equilibrium and at time t, respectively.

The constants, k_1 and q_e, in the experiment were calculated using the slope and intercept of plots of $\log(q_e - q_t)$ *versus* t (Table 2, Fig. 5A). The fit lines at each Mg/Si ratio yielded relatively low R_1^2 values and the experimental observations suggests that application of the equation is inappropriate as

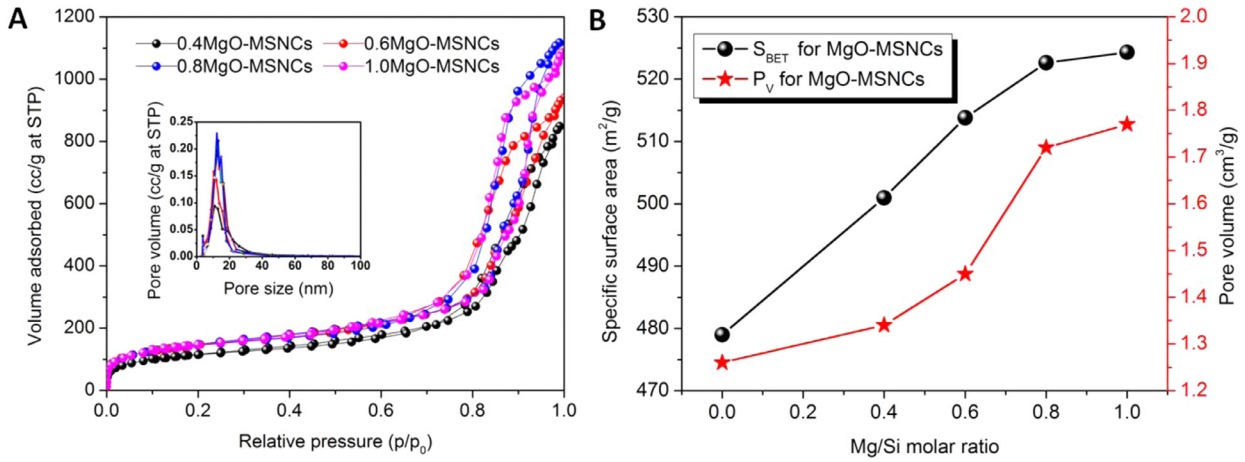

Fig. 3 – (A) Nitrogen adsorption desorption isotherms and pore size distributions (the inset) of MgO-MSCNs with different molar ratios; (B) Specific surface area and pore volume changes at different molar ratios for MgO-MSNCs.

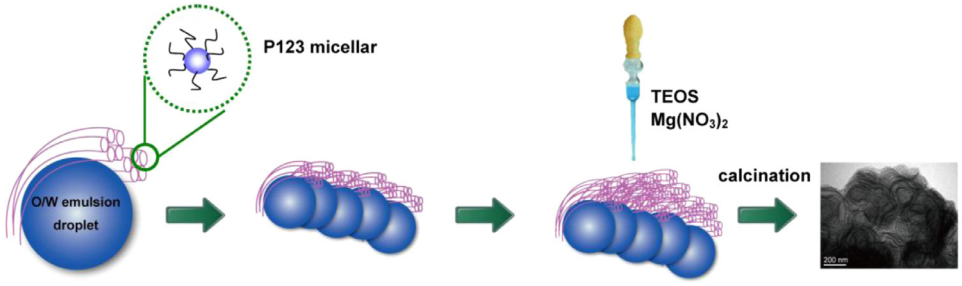

Scheme 1 – Schematic illustration of the in-situ emulsion-assisted process of MgO-MSNCs.

Table 2 – Adsorption kinetic model rate constants for IMC adsorption on MgO-MSCNs.

Sample	$q_{e,exp}$ (mg/g)	First-order			Second-order		
		k_1 (min)	$q_{e,cal}$ (mg/g)	R_1^2	$k_2 \times 10^{-3}$ (g/mg/min)	$q_{e,cal}$ (mg/g)	R_2^2
MSNCs	28.34	0.0067	7.99	0.83633	7.44	27.32	0.9992
0.4MgO-MSNCs	36.71	0.0090	8.87	0.7431	6.14	34.01	0.9965
0.6MgO-MSNCs	40.65	0.0113	10.45	0.7314	7.71	35.71	0.9993
0.8MgO-MSNCs	50.84	0.0124	11.73	0.7937	8.22	49.02	0.9992
1.0MgO-MSNCs	67.94	0.0193	43.17	0.9742	8.15	71.43	0.9784

the experimental observations are nonlinear when plotted in this manner. In addition, the agreement between the experimentally observed equilibrium adsorption and that derived using Eq. (2) is poor. This suggests that the adsorption of IMC on MgO-MSCNs did not follow pseudo-first-order kinetics.

The pseudo-second-order rate expression [18] can be linearly expressed as:

$$t/q_t = 1/k_2 q_e^2 + t/q_e \quad (3)$$

Where k_2 is the rate constant for pseudo-second-order adsorption (g/mg/h) and $k_2 q_e^2$ or h (mg/g/h) is the initial adsorption rate.

The experimental values of the solid phase concentration of adsorbate at equilibrium ($q_{e,exp}$) and the calculated value of the solid phase concentration of adsorbate at equilibrium ($q_{e,calc}$) for the pseudo-second-order models are also shown in Table 2 and Fig. 5B. Shows that the fitted equilibrium adsorption capacities derived from Eq. (3) are similar at each molar ratio and in close agreement with those observed experimentally, and also, the calculated correlation coefficients (R_2^2) are also closer to unity of pseudo-second-order kinetics. Therefore, the IMC adsorption by MgO-MSCNs can be more appropriately described by the pseudo-second-order kinetic model and IMC is adsorbed onto MgO-MSCNs via a chemical interaction.

3.3. *Adsorption isotherms*

Various adsorption isotherm equations were used to describe the equilibrium nature of adsorption. The Freundlich isotherm is suitable for highly heterogeneous surfaces, while

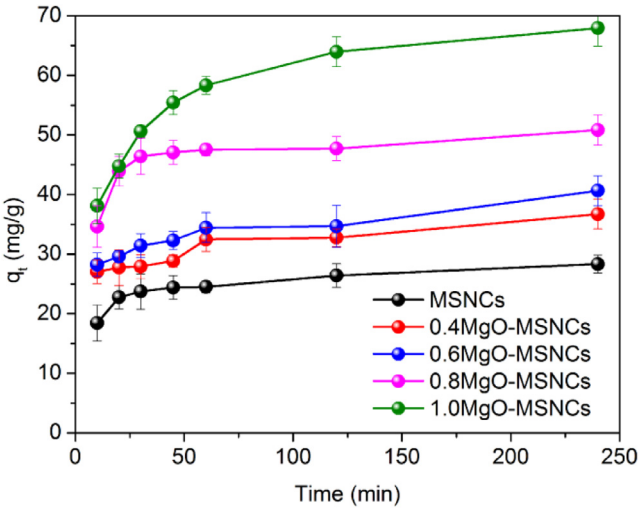

Fig. 4 – Effect of molar ratio of Mg/Si on the adsorption kinetics of IMC by MgO-MSCNs.

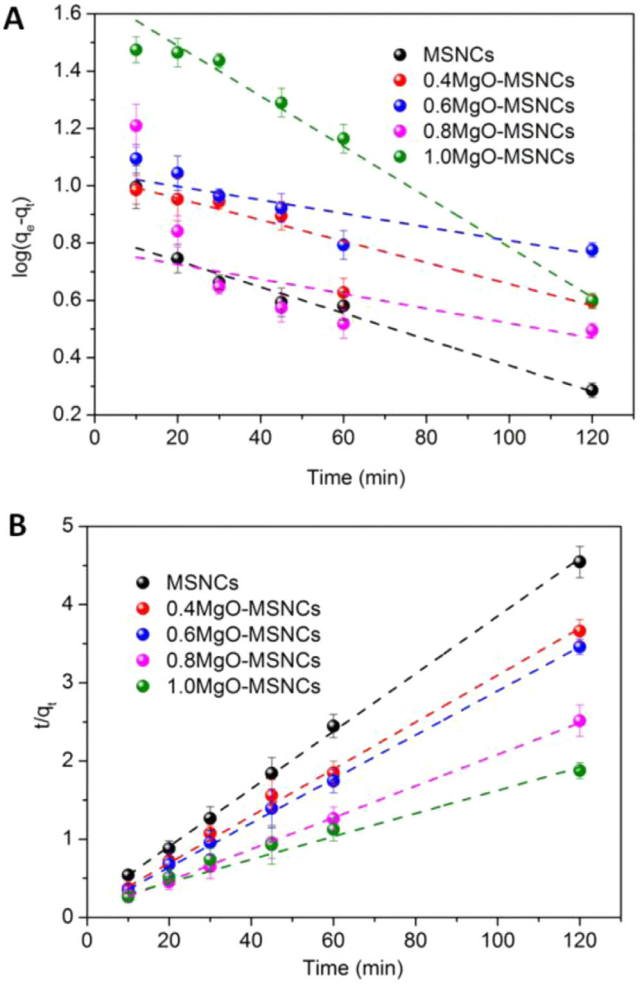

Fig. 5 – (A) Pseudo first-order kinetic and (B) pseudo second-order kinetic model fit for IMC sorption onto MgO-MSCNs at various molar ratios ($n = 3$).

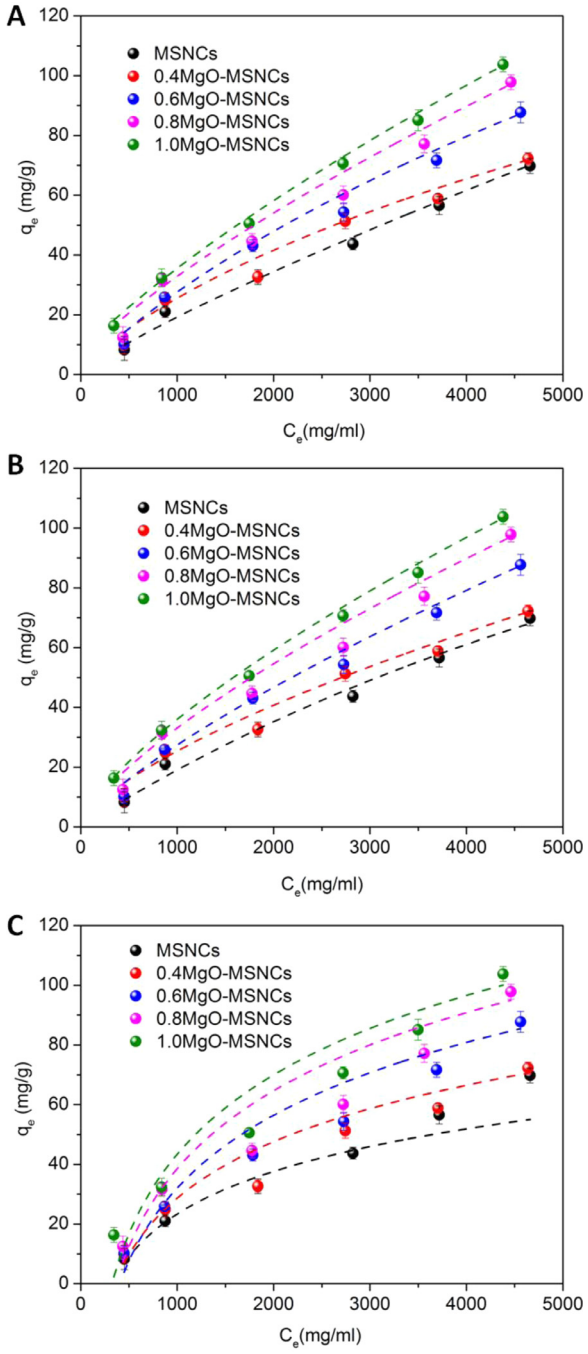

Fig. 6 – (A) Freundlich, (B) Langmuir and (C) Temkin isotherms for IMC adsorption on MgO-MSCNs ($n = 3$).

the Langmuir equation [19] is valid for homogeneous surfaces. Regarding the Temkin isotherm, this takes into accounting the interactions between the adsorbing material and the adsorbate. The isotherm assumes that the heat of adsorption of the molecules decreases linearly with coverage due to their interactions and the adsorption is characterized by a uniform distribution of binding energies [20].

In this experiment, the adsorption of IMC by MgO-MSCNs was modeled using the Freundlich (Fig. 6A), Langmuir (Fig. 6B), and Temkin isotherms (Fig. 6C). The isotherm

Table 3 – Langmuir, Freundlich, and Temkin isotherm model parameters and correlation coefficients for adsorption of IMC on MgO-MSCNs.

Isotherm	Sample	Parameters		
		k_F	n	R^2
Freundlich	MSNCs	0.074	1.24	0.9895
	0.4MgO-MSNCs	0.135	1.35	0.9880
	0.6MgO-MSNCs	0.118	1.29	0.9568
	0.8MgO-MSNCs	0.148	1.09	0.9747
	1.0MgO-MSNCs	0.196	1.34	0.9926
Langmuir	Sample	q_m (mg/g)	$k_L \times 10^5$ (l/mg)	R^2
	MSNCs	177.58	8.83	0.9848
	0.4MgO-MSNCs	233.29	10.42	0.9798
	0.6MgO-MSNCs	237.11	11.43	0.9595
	0.8MgO-MSNCs	238.26	12.86	0.9612
	1.0MgO-MSNCs	275.44	13.01	0.9868
Temkin	Sample	$k_T \times 10^3$	b	R^2
	MSNCs	2.67	24.51	0.9301
	0.4MgO-MSNCs	2.92	25.10	0.9307
	0.6MgO-MSNCs	2.79	29.42	0.9091
	0.8MgO-MSNCs	2.86	31.10	0.8802
	1.0MgO-MSNCs	3.76	32.20	0.8970

constants and the correlation coefficient (R^2) with the experimental data are listed in Table 3.

The Freundlich isotherm is suitable for both monolayer and multilayer adsorption, and it is based on the assumption that the adsorbate is adsorbed on the heterogeneous surface of an adsorbent [21]. The linear form is expressed as:

$$\log q_e = \log K_F + \log C_e/n \quad (6)$$

Where K_F and n are Freundlich isotherm constants related to the adsorption capacity and adsorption intensity, respectively and C_e is the equilibrium concentration (mg/l).

The Freundlich isotherm constants K_F and $1/n$ represent the adsorption capacity and adsorption intensity, respectively. Since the n values are greater than one, this indicates that the affinity between the adsorbate and adsorbent is high. In other words, IMC is well adsorbed by MgO-MSNCs. The high correlation coefficients (R^2) indicate that the interaction between the two materials is one of chemisorption.

Since the Freundlich isotherm does not predict the saturated adsorption capacity of the adsorbent surface by the adsorbate. So, the maximum adsorption capacity of adsorbent (q_m) is calculated by the Langmuir isotherm equation.

The Langmuir isotherm assumes that only monolayer adsorption can occur on the surface of the adsorption sites. Once a site is filled, no other sorption can take place at that position. When the surface eventually reaches saturation, the maximum adsorption will be obtained. The Langmuir isotherm model is described as:

$$C_e/q_e = 1/K_L q_m + C_e/q_m \quad (5)$$

Where K_L is the Langmuir constant related to the energy of adsorption and q_m is the maximum adsorption capacity (mg/g) [21].

Table 4 – Property characterization for drug carriers after drug loading.

Sample	D_p (nm)	S_{BET} (m^2/g)	V_t (cm^3/g)	Loading content (%)
MSNCs	<2	102.90	0.73	12.95 ± 1.23
0.4MgO-MSNCs	<2	87.63	0.57	14.88 ± 0.97
0.6MgO-MSNCs	<2	35.80	0.30	15.75 ± 1.01
0.8MgO-MSNCs	<2	18.10	0.18	18.95 ± 0.59
1.0MgO-MSNCs	<2	5.74	0.04	23.45 ± 0.77

The parameters of IMC adsorption on MgO-MSCNs were in good agreement with the observed behavior. In the equation, K_L indicates the affinity of IMC for the adsorbents, and the maximum adsorption capacity of IMC ranged from 177.58 mg/g to 275.44 mg/g with an increasing Mg/Si molar ratio.

The Temkin isotherm model assumes that the adsorption energy decreases linearly with the surface coverage. The linear form of the Temkin isotherm is:

$$q_e = RT \ln K_T/b + RT \ln C_e/b \quad (7)$$

Where b is the Temkin constant related to the heat of sorption (J/mol) and K_T is the Temkin isotherm constant (l/g) [22].

The Temkin isotherm model is also used to confirm whether the interaction between the adsorbate and the adsorbent is one of chemisorption [23]. From Table 3, the correlation coefficients (>0.90) demonstrated that the adsorption of IMC on MgO-MSCNs fitted quite well with the Temkin isotherm equation. This further supports the finding that the adsorption of IMC onto MgO-MSCNs particles was dominated by a chemisorption process.

3.4. *Drug loading and characterization*

In the drug loading process, IMC was incorporated into MgO-MSCNs samples by the adsorption equilibrium method. Methanol was selected as the solvent because of the good solubility of IMC in methanol. The drug loading amount was determined by UV spectrometry, and the results are listed in Table 4. The drug loading amount of IMC in five different carriers increased with an increasing of Mg/Si molar ratio, which was in agreement with the results of adsorption kinetics experiments. The surface areas and pore size of the obtained carriers were significantly reduced after drug loading. Because the basicity of the carrier enhanced with the increase of MgO doping ratio in composites, and the binding force with the acidic drug was also increased. The larger space of the carrier surface and the channel occupied by the drug IMC, the smaller surface area of the carrier after drug loading.

The morphology of the drug-loaded samples was studied by TEM as shown in Fig. S2. Compared with unloaded MgO-MSCNs samples, most of the pore channels were not clear, indicating that a large number of the pore channels had been filled with IMC. In addition, the diameter and PDI of IMC-1.0MgO-MSCNs was 1127 nm with a PDI of 0.306, which was similar to that of 1.0MgO-MSCNs.

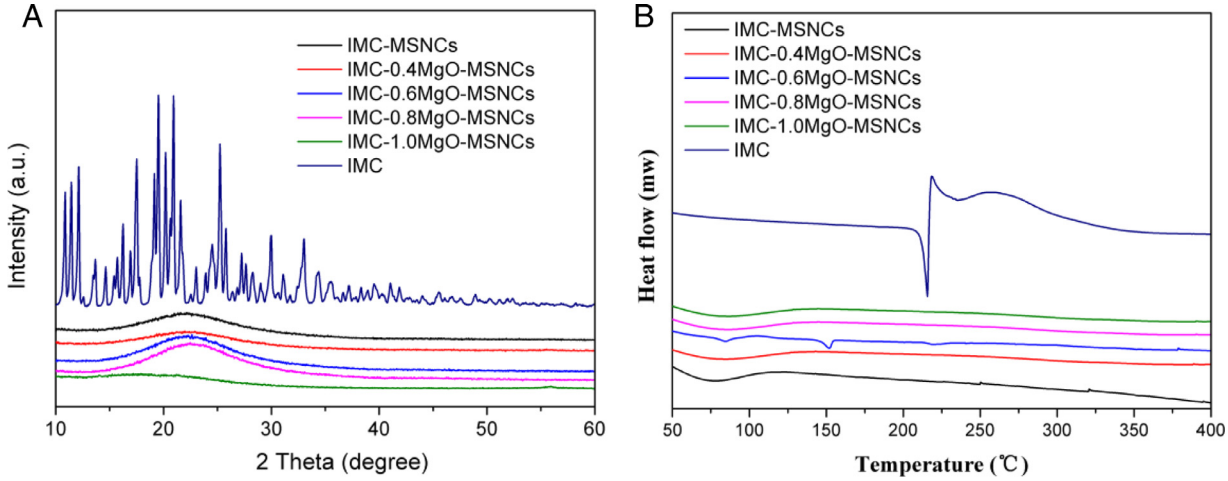

Fig. 7 – (A) XRD pattern and (B) DSC profiles of IMC, IMC-MSNCs, IMC-0.4MgO-MSNCs, IMC-0.6MgO-MSNCs, IMC-0.8MgO-MSNCs and IMC-1.0MgO-MSNCs.

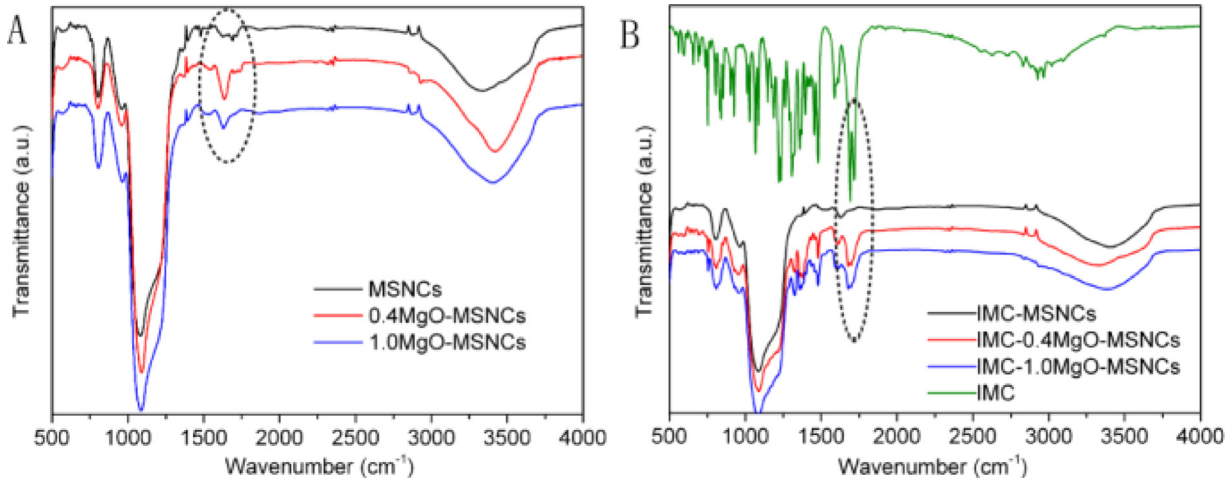

Fig. 8 – FTIR spectra of (A) MSNCs and MgO-MSNCs, and (B) IMC encapsulated in MSNCs and MgO-MSNCs.

The physical state of IMC in MgO-MSNCs was characterized by XRD and DSC. Powder samples were scanned over the 2θ angle range from 10° to 60°, and XRD result is shown in Fig. 7A. The raw IMC showed intense and characteristic crystalline diffraction peaks at 2θ = 11.4°, 17.5°, 19.5°, 21.6° and 25.2°. However, no distinctive crystalline peaks of the drug were observed after the drug loaded into the mesoporous MgO-MSNCs composite, indicating that the drug loaded in the carrier was in an amorphous state. DSC measurements were used to further verify the physical state of IMC. As shown in Fig. 7B, IMC raw drug has a sharp melting point, however, there was no endothermic peak in the range of 50–400 °C in IMC loaded samples. The results showed that the drug can be completely loaded into the inner channel of the carrier, and the drug was in an amorphous state, which is consistent with the results of XRD.

FTIR spectrum can also provide the evidence of anion complexion with cation in the sample of MSNCs and MgO-MSNCs as shown in Fig. 8A. The peaks at 1090.8 and 804.0 cm^{-1} of unmodified mesoporous MSNCs were because of the asymmetric and symmetric stretching of Si–O–Si lattice vibrations, respectively. The peaks at 1634.6 and 960.6 cm^{-1} were attributed to Si–OH. After the MSNCs were assembled by MgO, the characteristic peak of Si–OH at 1634.6 cm^{-1} became stronger with increasing MgO simultaneously. It could be explained as follows, with the increasing of MgO content, the number of water molecules interacting with the Si–O–Si of MSNCs was also increased in order to form the surface hydroxyls. When the MgO ratio rises to 1.0, the peak began to decrease. This phenomenon may be explained by the surface hydroxyls beginning to release H^+, which leading to decreased amounts of the surface hydroxyls.

To get a better understanding of the intercalation mode between the IMC drugs and the prepared silica matrix, the FTIR spectrum was also used to describe the possible intermolecular interactions, as depicted in Fig. 8B. The characteristic peaks of pure IMC were 1717.6 and 1691.4 cm^{-1}, which were corresponding to the carbonyl group of the acid and

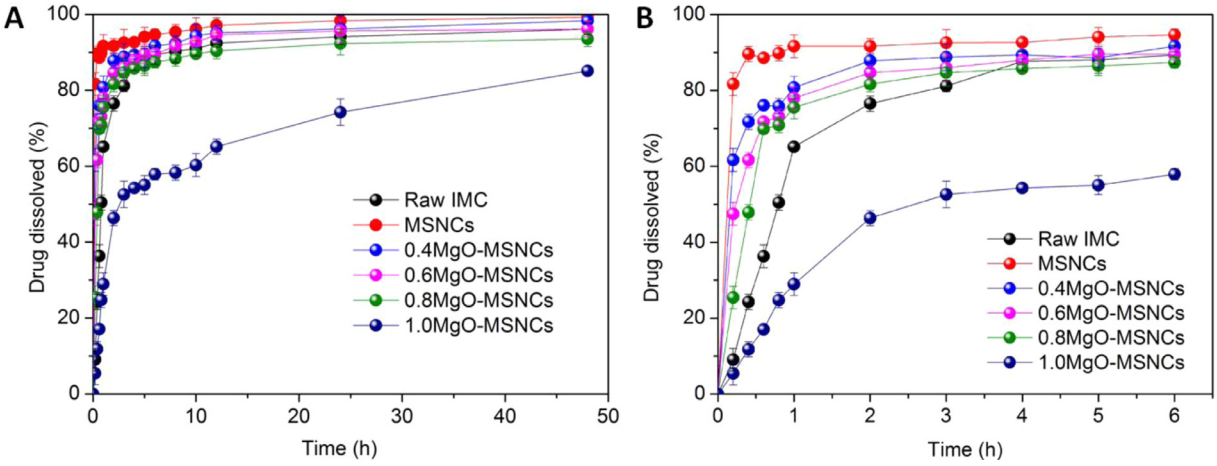

Fig. 9 – Dissolution profiles of MgO-MSNCs with different molar ratios and raw IMC (A) 48 h and (B) 6 h.

amide, respectively. In contrast, when the IMC-loaded silica were formulated, the originally carbonyl stretching peaks became weaker and broader, and shifted to lower wave numbers of 1705 and 1678 cm^{-1}, respectively. This phenomenon indicated that the acid and amide functional groups of IMC were reacted with the hydroxyl of the silica surface. Some researchers have been published on the interactions between acid drug molecules and unmodified or MgO modified silica matrices, wherein the hydroxyl group on the surface of silica tends to interact with the carbonyl group of the drug [12]. The FTIR results confirmed that IMC have been successfully loaded into the obtained mesoporous silica materials.

3.5. *In vitro release profiles*

In vitro release tests were carried out to study the application of MgO-MSCNs as a drug carrier and to investigate the effect of different Mg/Si ratios of samples on the dissolution behavior of IMC. The release of IMC from MgO-MSCNs mainly involved two stages: burst release and slow release. The reason for the initial burst release was probably due to the fact that the drug is present in the outer pores of mesoporous materials. As shown in Fig. 9(A) and (B), the release rate of IMC from pure MSNCs was much faster than that from raw IMC. Since IMC is a BCS class II drug, the dissolution rate of IMC within 1 h was about 65% because of its poor dissolution. So, the most likely reason for the improved dissolution may be the spatial confinement of the MSNCs pores, which reduced the degree of IMC crystallization and maintained the drug in a non-crystalline state, which effectively increased the dissolution rate. Because of the addition of swelling agents, MSCNs have relatively larger pores (9.79 nm), and the spacious pore channels means they encounter less diffusion resistance and escape more easily into the dissolution medium. The whole release process of the drug molecules involves the drug dissolving in the dissolution medium and escaping from the pore channels. Therefore, larger pores allow the dissolution medium to penetrate more easily into the carriers pore channels, and the drug molecules would have more chance of being released from the carriers. So, it could be predicted that MSNCs could significantly increase the release rate of poorly water-soluble drugs owing to their large pores and open pore structure.

In Fig. 9A and B, the release rates of IMC from MgO-MSCNs samples were slower with an increase in the Mg/Si ratio. The dissolution rate of IMC from the Mg/Si = 1 sample within 1 h was only about 29%, while the Mg/Si = 0 sample had a release rate of IMC of 92%. In the first 6 h, 95% of the IMC was released from the Mg/Si = 0 sample, and the cumulative release of IMC from Mg/Si = 1 sample was 57%. After 6 h, the release rate slowed down. The maximum amount of IMC released is 85% and 99% within 48 h, respectively. The different dissolution rates can be attributed to the formation of stronger bonds between the acidic IMC drugs and basic samples compared with those between the drugs and MgO-MSCNs. With the increasing Mg/Si ratio, the amount of the surface hydroxyl was higher, IMC with the carbonyl group of the acid and amide was apt to interact with the surface of the carriers and, so the interaction between them is greater, which results in a slower release rate. Since all the five carriers possess a similar morphology, the pore size may also influence the release rate. However, to our surprise, the larger pore size of Mg/Si = 1 did not markedly influence the rate of drug release. In our drug delivery system, the combination of an acidic drug and alkaline carriers plays the most important role.

3.6. *In vitro cell cytotoxicity evaluation*

The results of MTT assays in Fig. 10 indicated that both MSCNs and MgO-MSCNs exhibited negligible cytotoxicity on Caco-2 cells at tested concentrations. Even at the highest concentration of 500 μg/ml, cell viability was higher than 85%. The negligible cell cytotoxicity of MgO-MSCNs against Caco-2 cells might due to the relatively large particle size which was hardly to be uptake by the cells. These results indicated that MSCNs and MgO-MSCNs could be used as the safe carriers for oral drug delivery.

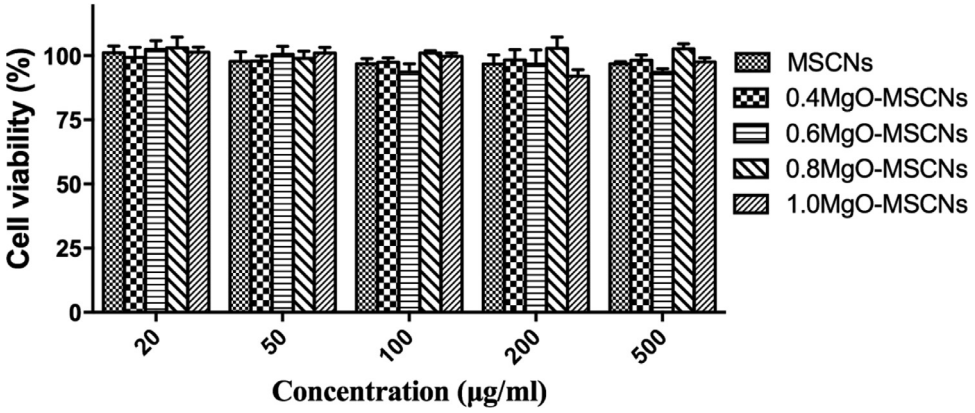

Fig. 10 – Effect of MSNCs and MgO-MSNCs on cell viability of Caco-2 cells by MTT assay.

4. Conclusion

In summary, the novel ordered mesoporous MgO-modified mesoporous silica cocoons (MgO-MSNCs) with different Mg/Si molar ratio were prepared to encapsulate the acidic drugs. The adsorption was found to be strongly dependent on the Mg/Si molar ratio. The IMC adsorption rate and the maximum adsorption capacity with the increase of Mg/Si molar ratio. And the adsorption kinetics could be accurately described by the pseudo-second-order kinetic model. The Freundlich isotherm produced a good fit, indicating that the coverage of the MgO-MSNCs surface with IMC was heterogeneous. The maximum adsorption capacity of adsorbent is calculated by the Langmuir isotherm equation. The experimental data also fitted the Temkin equation well, which further supports the hypothesis that the IMC adsorption on MgO-MSNCs was dominated by a chemisorption process. Since MgO-MSNCs samples have a stronger affinity for drug molecules compared with pure MSNCs, MgO-MSNCs have the advantage of adjusting the drug release rate of IMC. We also believe that our research on MgO-MSNCs carriers highlights the potential therapeutic benefits associated with the safe and effective management of the acidic drug adsorption and *in vitro* release.

Acknowledgment

This work was supported by the National Basic Research Program of China (973 Program) (No. 2015CB932100), National Natural Science Foundation of China (No. 81473165) and Liaoning Provincial Key Laboratory of Drug Preparation Design & Evaluation of Liaoning Provincial Education Department (No. LZ2015068).

Conflicts of interest

The authors declare that there are no conflicts of interest.

Supplementary materials

Supplementary material associated with this article can be found, in the online version, at doi:10.1016/j.ajps.2018.08.004.

REFERENCES

[1] Slowing I, Vivero-Escoto J, CwLin V. Mesoporous silica nanoparticles as controlled release drug delivery and gene transfection carriers. Adv Drug Deliv Rev 2008;60(11):1278–88.
[2] Vallet-Regi M, Rámila A, Real RPD, Pérez-Pariente J. A new property of mcm-41: drug delivery system. Chem Mater 2001;13(2):308–11.
[3] Zhao QF, Liu J, Zhu W, et al. Dual-stimuli responsive hyaluronic acid-conjugated mesoporous silica for targeted delivery to CD44-overexpressing cancer cells. Acta Biomater 2015;23:147–56.
[4] Zhang H, Wang YM, Lü K, et al. Hierarchical fabrication of silica cocoon with hexagonally ordered channel constructed wall via an emulsion-assisted process. Microporous Mesoporous Mater 2012;150(1):90–5.
[5] Blin JL, Otjacques C, Herrier G, Su BL. Pore size engineering of mesoporous silicas using decane as expander. Langmuir 2000;16(9):4229–36.
[6] Zhou G, Chen Y, Yang J, Yang S. From cylindrical-channel mesoporous silica to vesicle-like silica with well-defined multilamella shells and large inter-shell mesopores. J Mater Chem 2007;17(27):2839–44.
[7] Vialpando M, Backhuijs F, Martens JA, Mooter GVD. Risk assessment of premature drug release during wet granulation of ordered mesoporous silica loaded with poorly soluble compounds itraconazole, fenofibrate, naproxen, and ibuprofen. Eur J Pharm Biopharm 2012;81(1):190–8.
[8] Li X, Yan Y, Lin Y, et al. Hollow mesoporous carbon as a near-infrared absorbing carrier compared with mesoporous carbon nanoparticles for chemo-photothermal therapy. J Colloid Interface Sci 2017;494:159–69.
[9] Sun L, Wang Y, Jiang T, et al. Novel chitosan-functionalized spherical nanosilica matrix as an oral sustained drug delivery system for poorly water-soluble drug carvedilol. J Control Release 2013;5(1):103–13.
[10] Wei YL, Cao Y, Zhu JH. Attempts on preparing mesoporous basic material MgO/SBA-15. Stud Surface Sci Catal 2004;154(4):878–85.

[11] Wang R, Liu XW, He Y, et al. The humidity-sensitive property of mgo-sba-15 composites in one-pot synthesis. Sensor Actuat B-Chem 2010;145(1):386–93.
[12] Alexa IF, Ignat M, Popovici RF, Timpu D, Popovici E. *In vitro* controlled release of antihypertensive drugs intercalated into unmodified sba-15 and mgo modified sba-15 matrices. Int J Pharm 2012;436(1–2):111–19.
[13] Shen S, Chow PS, Chen F, Tan RB. Submicron particles of SBA-15 modified with MgO as carriers for controlled drug delivery. Chem Pharm Bull (Tokyo) 2007;55(7):985–91.
[14] Benguella B, Benaissa H. Cadmium removal from aqueous solutions by chitin: kinetic and equilibrium studies. Water Res 2002;36(10):2463–74.
[15] Wang YM, Wu ZY, Wei YL, Zhu JH. In situ coating metal oxide on sba-15 in one-pot synthesis. Microporous Mesoporous Mater 2005;84(1):127–36.
[16] Li ZZ, Katsumi T, Imaizumi S, Tang XW, Inui T. Cd(II) adsorption on various adsorbents obtained from charred biomaterials. J Hazard Mater 2010;183(1):410–20.
[17] Ho YS. Citation review of Lagergren kinetic rate equation on adsorption reactions. Scientometrics 2004;59(1):171–7.
[18] Ho Y-S. Review of second-order models for adsorption systems. ChemInform 2006;136(3):681–9.
[19] Calvet R. Adsorption of organic chemicals in soils. Environ Health Persp 1989;83(4):145–77.
[20] Biggar JW, Cheung MW. Adsorption of picloram (4-amino-3,5,6-trichloropicolinic acid) on panoche, ephrata, and palouse soils: a thermodynamic approach to the adsorption mechanism. Soil Sci Soc Am J 1973;37(6):863–868.
[21] Tan G, Dan X. Adsorption of cadmium ion from aqueous solution by ground wheat stems. J Hazard Mater 2009;164(2):1359–63.
[22] Çelebi O, Üzüm Ç, Shahwan T, Erten HN. A radiotracer study of the adsorption behavior of aqueous Ba(2+) ions on nanoparticles of zero-valent iron. J Hazard Mater 2007;148(3):761–7.
[23] Biswas K, Saha SK, Ghosh UC. Adsorption of fluoride from aqueous solution by a synthetic iron(III)−aluminum(III) mixed oxide. Ind Eng Chem Res 2007;46(16):5346–5356.